Nanoscale

Check for updates

Giant coercivity enhancement in a room-temperature van der Waals magnet through substitutional metal-doping

Hyo-Bin Ahn, [ID] †[a] Soon-Gil Jung, [ID] †[b] Hyungjong Lim,[c] Kwangsu Kim,[d,e] Sanghoon Kim,[d] Tae-Eon Park,[e] Tuson Park*[f,g] and Changgu Lee [ID] *[a,c]

Fe_xGeTe_2 (x = 3, 4, and 5) systems, two-dimensional (2D) van der Waals (vdW) ferromagnetic (FM) metals with high Curie temperatures (T_C), have been intensively studied to realize all-2D spintronic devices. Recently, an intrinsic FM material Fe_3GaTe_2 with high T_C (350–380 K) has been reported. As substitutional doping changes the magnetic properties of vdW magnets, it can be a powerful means for engineering the properties of magnetic materials. Here, the coercive field (H_c) is substantially enhanced by substituting Ni for Fe in $(Fe_{1-x}Ni_x)_3GaTe_2$ crystals. The introduction of a Ni dopant with x = 0.03 can enhance the value of H_c up to ~200% while maintaining the FM state at room temperature. As the doping level increases, T_C decreases, whereas H_c increases up to 7 kOe at x = 0.12, which is the highest H_c reported so far. The FM characteristic is almost suppressed at x = 0.68 and a spin glass state appears. The enhancement of H_c resulting from Ni doping can be attributed to domain pinning induced by substitutional Ni atoms, as evidenced by the decrease in magnetic anisotropy energy in the crystals upon Ni doping. Our findings provide a highly effective way to control the H_c of the 2D vdW FM metal Fe_3GaTe_2 for the realization of Fe_3GaTe_2 based room-temperature operating spintronic devices.

Introduction

Substitutional doping of van der Waals (vdW) magnets can effectively tune their magnetic properties. In particular, in metallic ferromagnetic (FM) materials, substitutional doping not only alters the intrinsic magnetic properties, such as saturation magnetization (M_s), anisotropy field (H_k), and Curie temperature (T_C), but may also affect micro-magnetic characteristics, such as domain motion and domain wall energy.[1–7] For this reason, the effect of substitutional doping on vdW magnets cannot be understood in a simple way, but various aspects should be considered to precisely analyze the

outcome. Substitutional doping of Fe_xGeTe_2 (x = 3, 4, and 5), which are metallic FM materials, has been intensively researched because of their comparatively high T_C (Fe_3GeTe_2 ~ 220 K, Fe_4GeTe_2 ~ 280 K, Fe_5GeTe_2 ~ 300 K) and tunable material properties.[1–18] Their magnetic properties are shown to be modulated with substitutional doping, when the Fe atom is replaced with other transition metals such as Co and Ni.[2,4–7] In the case of $(Fe_{1-x}Co_x)_3GeTe_2$, substitutional doping detrimentally affects the T_C of crystals.[5] It has been reported that $(Fe_{1-x}Co_x)_3GeTe_2$ crystals, with doping ratios ranging from x = 0 to 0.58, exhibit pinning-type FM characteristics. The value of H_c at x = 0 is 0.2 kOe and H_c reaches a maximum value of approximately 1.5 kOe at x = 0.58. Despite having the highest H_c reported in vdW FM materials so far, the significant decrease in T_C means that the Co-doping on Fe_3GeTe_2 may not be advantageous for device application or commercialization purposes.

Diverse vdW FM materials have been studied since the discovery of 2D magnetism.[19–25] Recently, Zhang *et al.* have reported on the observation of intrinsic ferromagnetism in vdW Fe_3GaTe_2, which shows a T_C above room temperature (350–380 K), leading to the potential for the realization of room-temperature operating vdW spintronic devices.[26] It has an identical crystal structure to that of Fe_3GeTe_2, that is, the hexagonal space group $P6_3/mmc$. The difference in the crystal

[a]*SKKU Advanced Institute of Nanotechnology, Sungkyunkwan University, Suwon 16419, Korea*

[b]*Department of Physics Education, Sunchon National University, Suncheon 57922, Korea*

[c]*School of Mechanical Engineering, Sungkyunkwan University, Suwon 16419, Korea. E-mail: peterlee@skku.edu*

[d]*Department of Physics, University of Ulsan, Ulsan 44619, Korea*

[e]*Center for Spintronics, Korea Institute of Science and Technology, Seoul 02792, Korea*

[f]*Center for Quantum Materials and Superconductivity (CQMS), Sungkyunkwan University, Suwon 16419, Korea. E-mail: tp8701@skku.edu*

[g]*Department of Physics, Sungkyunkwan University, Suwon 16419, Korea*

† These authors equally contributed to this work.
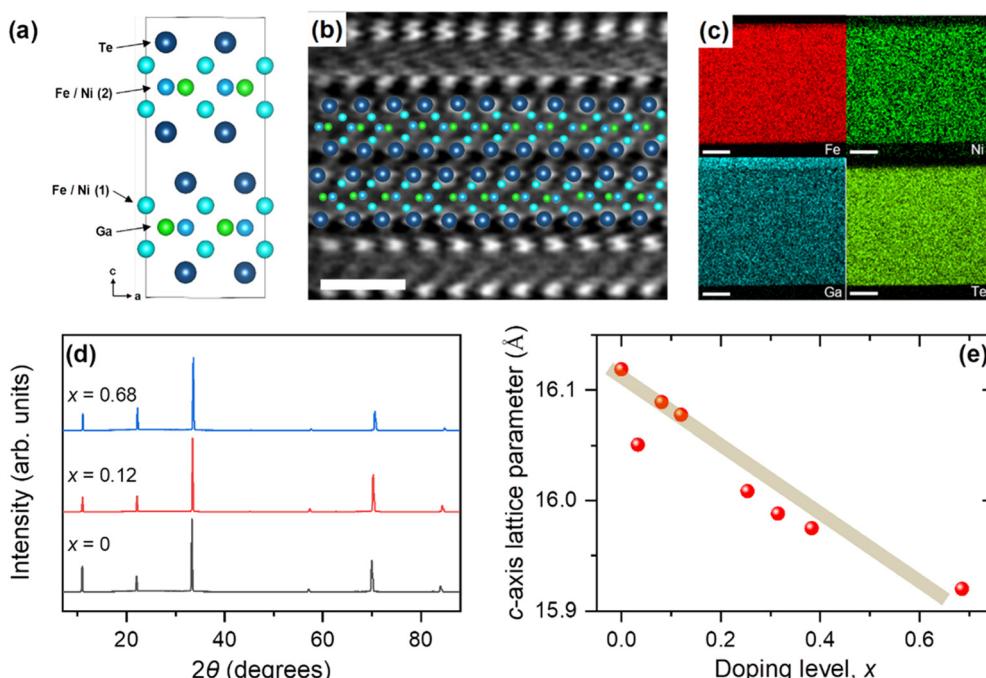
Fig. 1 Crystalcharacterization of doped FNGT. (a) Schematic of the layered structure of FNGT. (b) The cross-sectional scanning tunneling electron microscopy (STEM) image of FNGT with $x = 0.12$ (scale bar = 1 nm). (c) Tunneling electron microscopy (TEM) energy dispersive spectroscopy (EDS) mapping data of the crystal with $x = 0.12$ (scale bar = 100 nm). (d) Single crystal X-ray diffraction (XRD) patterns of selected FNGT with $x = 0$, 0.12, and 0.68, respectively. (e) c-Lattice parameter of FNGT with $x = 0$–0.68 obtained from the single crystal XRD patterns.

structure is the replacement of the Ge atom with a Ga atom and, consequently, the changes in bond lengths between atoms and crystal lattice parameters. The magnetic characteristics of Fe_3GaTe_2 are comparable to those of Fe_3GeTe_2, showing intrinsic ferromagnetism and large perpendicular magnetic anisotropy (PMA) below T_C. Control of the magnetic properties of FM materials is of high interest in spintronic applications, and the magnetic characteristics of Fe_3GeTe_2 are reported to be modulated by charge control methods such as electrical gating, current control, doping, *etc.*[2–9,13] Substitutional doping is one of the reported methods to tune the magnetic properties. However, it is hard to speculate on the effects of substitutional doping on metallic vdW FM materials because the results obtained so far have been inconsistent and varied.[2–6] Therefore, systematic investigation is needed to determine the effects of substitutional dopants on Fe_3GaTe_2 crystals in various combinations.

Here we report a remarkable enhancement of the H_c of $(Fe_xNi_{1-x})_3GaTe_2$ (FNGT) single crystals with $x = 0$–0.68. Our results suggest that the magnetic properties of FNGT crystals are strongly influenced by Ni substitution. We find that the Ni substitution can increase the H_c of FNGT from 0.6 kOe ($x = 0$) to 7.0 kOe ($x = 0.12$), which is caused by the domain pinning effect. To the best of our knowledge, this is the highest H_c among those reported for vdW FM materials so far. As the doping ratio increases further, their T_C and M_s gradually decrease. When the Fe atom is fully replaced with Ni (Ni_3GaTe_2), it becomes paramagnetic (PM).[27] Compared to the

$(Fe_{1-x}Co_x)_3GeTe_2$ case, higher H_c and T_C have been achieved. The enhancement of H_c in FM materials is desirable for increasing the thermal stability in memory applications and reducing the possibility of errors in device applications, which could potentially accelerate the commercialization of Fe_3GaTe_2.

Experimental methods

FNGT crystals have been synthesized by the self-flux method. The precursor is a mixture of Fe, Ni powder, Ga lumps, and Te pellets in a molar ratio of $1 - x : x : 1 : 2$, and is inserted into a quartz ampoule. Te plays the role of flux. The ampoule is then evacuated and sealed while maintaining vacuum conditions. After sealing, it is placed into a box furnace, heated up to 1273 K in 24 hours and then kept for 24 hours for forming a homogeneous mixed state of the precursor. Then, it is cooled at a rate of 3 K per hour to 773 K and then rapidly cooled down to room temperature. A molar ratio of elements in FNGT with $x = 0$–0.68 is measured with scanning electron microscopy (SEM) energy dispersive X-ray spectroscopy (EDS). Single crystal X-ray diffraction (XRD) patterns in the *ab* plane were collected with a high resolution X-ray diffractometer using Cu K_α whose wavelength is 1.5406 Å. The magnetic characteristics of crystals are measured using a magnetic property measurement system (MPMS 5 T, Quantum Design).

Results and discussion

The crystal structure of the mother compound Fe_3GaTe_2 belongs to the space group of $P6_3/mmc$ with a hexagonal structure, and its unit cell consists of two vdW layers as shown in Fig. 1a and b.[26] Each Fe_3Ga layer is surrounded by Te terminals and Fe_3GaTe_2 layers are divided by a vdW gap. Fig. 1c and d present the transmission electron microscopy (TEM)

EDS mapping result of FNGT with $x = 0.12$ and the representative XRD results for single crystals with $x = 0$, 0.12, and 0.68, respectively. The SEM EDS result reveals that the molar ratio of the synthesized crystals is $(Fe + Ni) : Ge : Te = 2.91 : 1 : 1.99$. The homogeneous distribution of Fe–Ni atoms as presented in TEM EDS mapping and the XRD peaks indicate that Fe atoms are well replaced with Ni dopants while maintaining the original structure. The XRD peaks are indexed to $(00l)$. Fig. 1e
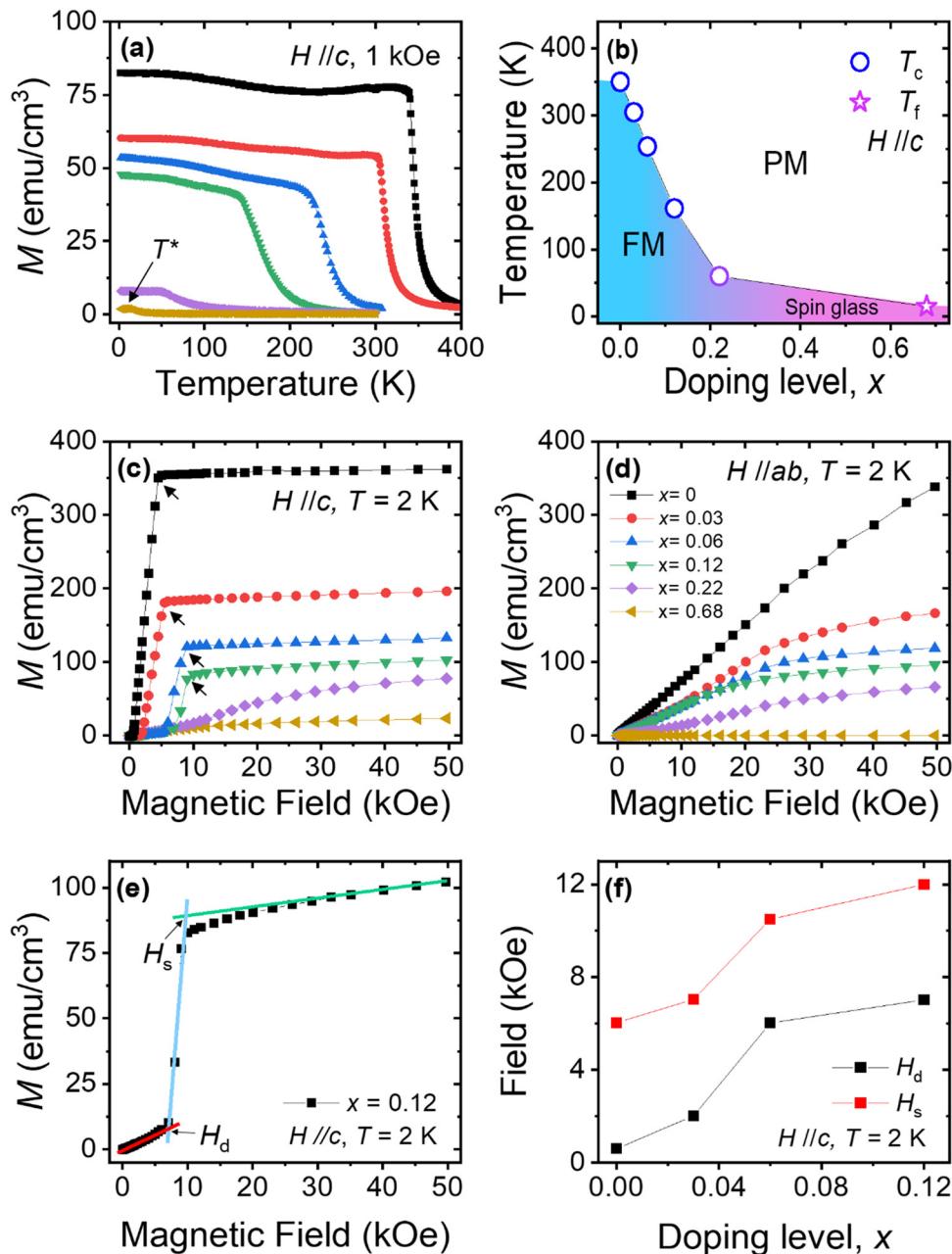
Fig. 2 Magnetic characteristics of FNGT. (a) Temperature-dependent magnetization ($M–T$) curves of FNGT with $x = 0–0.68$. (b) Transition temperature of FNGT. For FNGT with $x = 0–0.22$, the plotted transition temperature is the Curie temperature (T_C) as they show ferromagnetic (FM) characteristics. (c) Isothermal magnetization ($M–H$) curve of FNGT with $H//c$ measured at 2 K. Arrow pointed magnetization is the saturation magnetization (M_s) of each crystal. (d) $M–H$ curve of FNGT with $H//ab$ measured at 2 K. (e) $M–H$ curve of FNGT with $x = 0.12$, $H//c$ at 2 K. The red, blue, and green lines are linearly fitted curves in the pinning state, depinning state, and saturation state, respectively. H_d and H_s correspond to the depinning field and saturation field, respectively. (f) x dependence of H_d and H_s obtained from the $M–H$ curves of FNGT with $H//c$, 2 K.

shows the c-axis lattice parameter of FNGT with respect to the Ni doping level x obtained from XRD and TEM EDS data, indicating a gradual decrease of the c-axis lattice parameter as x increases.

To investigate changes in the magnetic properties of FNGT with respect to x, we performed temperature-dependent magnetization (M–T) measurements and isothermal magnetization hysteresis (M–H) measurements. Fig. 2a shows the temperature dependence of field-cooled (FC) magnetization (M) at 1 kOe

for FNGT, where the magnetic field was applied perpendicularly to the ab plane of the crystal ($H/\!/c$). FNGT with the Ni doping level $x = 0$–0.12 shows a clear FM transition, and both the T_C and magnitude of M gradually decrease as x increases. For FNGT with $x = 0.22$, the transition from PM to FM states weakens significantly, and for $x = 0.68$, it becomes ambiguous. The T_C of FNGT with $x = 0$–0.22 was estimated based on the Curie–Weiss law, and the transition temperature T^* for $x = 0.68$ was determined at the temperature of maximum M, as
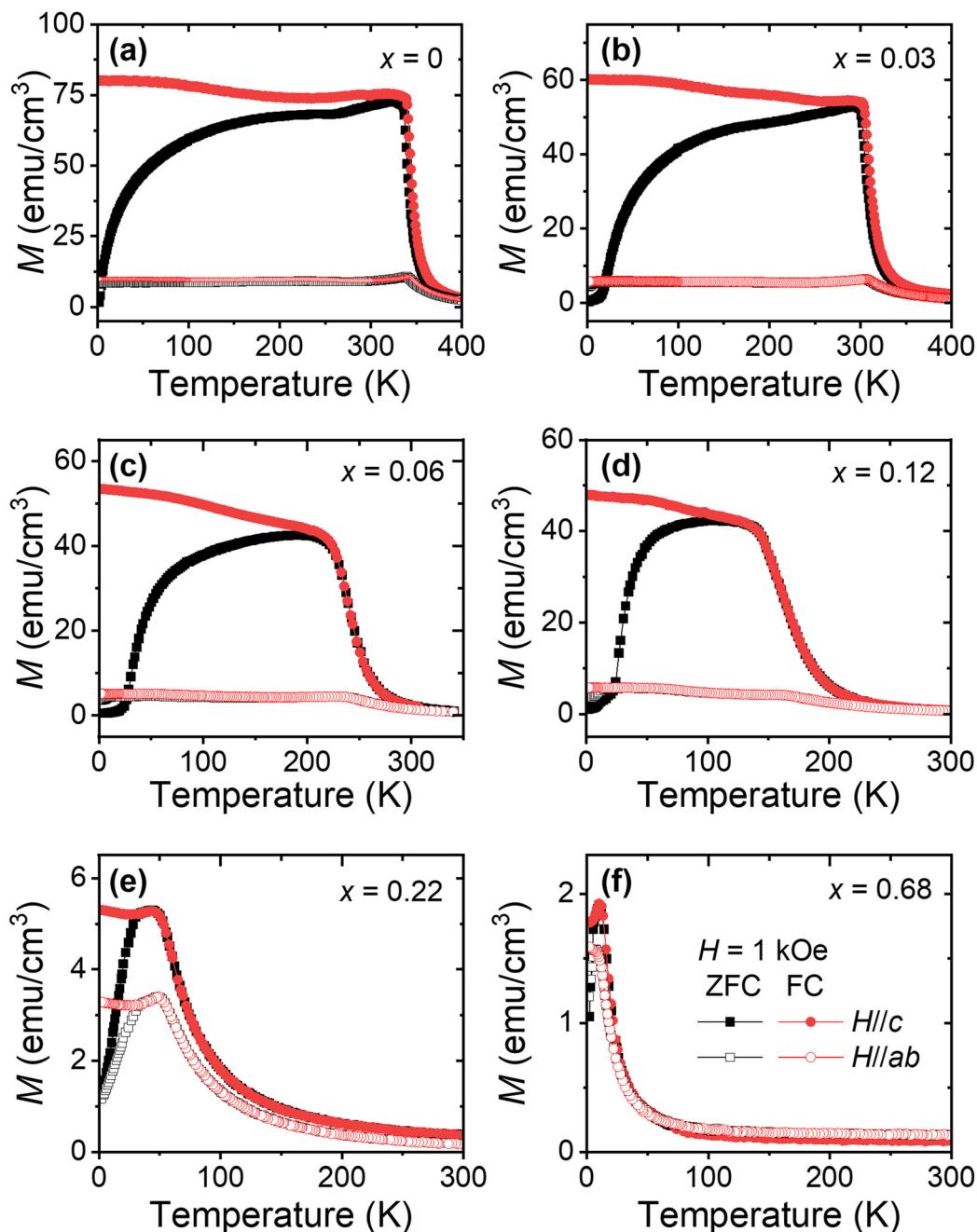

Fig. 3 Temperature-dependent magnetization curves of FNGT. (a–f) Field cooling (FC) and zero-field cooling (ZFC) temperature-dependent magnetization (M–T) curves of FNGT with $x = 0$–0.68 with $H/\!/c$ and $H/\!/ab$, $H = 1$ kOe.

indicated by the arrow in Fig. 2a. The obtained transition temperatures T_C and T^* from the M–T data are plotted in Fig. 2b. For FNGT with $x = 0.68$, T^* seems to be related to a spin-glass transition,[5,6] which will be discussed briefly in the latter part of this paper.

Fig. 2c and d present the zero-field-cooled (ZFC) M as a function of the applied magnetic field (M–H) at 2 K for FNGT for $H//c$ and $H//ab$, respectively. For FNGT with $x = 0$–0.12, the

difference between the M–H curve with $H//c$ and the M–H curve with $H//ab$ shows that these FNGT crystals have large PMA. For $x = 0$–0.12, as shown in Fig. 2c, M gradually increases at low fields and rapidly saturates at a particular field upon applying a high magnetic field. Until reaching the critical field, M remains nearly constant despite the increasing magnetic field. Specifically, the three-step M process can be clearly observed in the M–H curves of FNGT with $x = 0$–0.12 at 2 K (Fig. 2c),
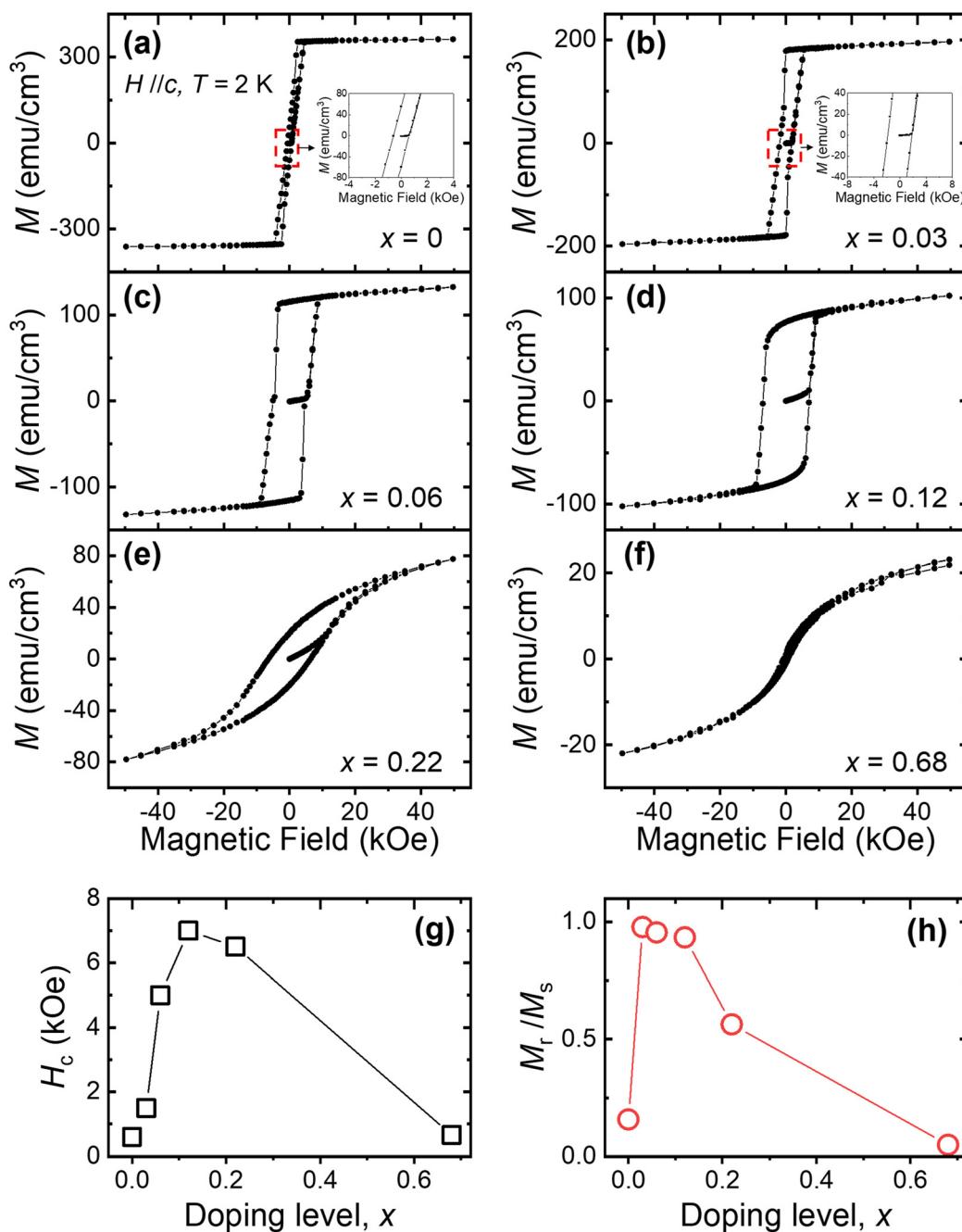
Fig. 4 Hysteresisloop of FNGT at 2 K. (a–f) Hysteresis loop of FNGT with $x = 0$–0.68. The field range is ±50 kOe. The insets in (a and b) are the magnification of the red-dashed area. (g) x dependence of coercive fields (H_c). (h) x dependence of the ratio of remanent magnetization (M_r) to saturation magnetization (M_s). Every H_c and M_r/M_s is obtained from Fig. 4a–f. All data are measured with $H//c$ at 2 K.

which is a typical behavior of pinning-type FM materials.[5,28,29] The depinning field (H_d) and the saturation field (H_s) can be determined from the M–H curves using a linear fit (Fig. 2e), and the dependence of these values on x is shown in Fig. 2f. We divided the M–H curves into three magnetic states: (i) domain pinning state, (ii) depinning state, and (iii) saturated state. As x increases, both H_d and H_s increase linearly, which implies that the Ni dopant plays a critical role as a domain wall pinning site that hinders domain propagation for flipping in three magnetic states. For FNGT with $x \geq 0.22$, however, this behavior becomes vague and the M–H curve gradually increases in the measured field range without the three-step M process observed with low x values (0–0.12), indicating the suppression of FM characteristics. These results are consistent with the M–T measurements in Fig. 2a.

The temperature dependence of FC M and ZFC M on both the directions $H\parallel c$ and $H\parallel ab$ for FNGT with $x = 0$–0.68 is plotted in Fig. 3a–f. The initial value of ZFC M for FNGT with $x = 0$–0.12 is nearly zero. As the temperature increases from 2 K, a steep increase of ZFC M occurs and it increases until a transition from FM to PM occurs. A similar behavior has been reported in previous works,[5,26,29] which is typically observed in Ising-type ferromagnetic materials due to multi-domain formation during cooling without an external field. In Fig. 3a, ZFC M drastically increases as the temperature increases monotonically below ~20 K. On the other hand, as shown in Fig. 3b–d, ZFC M is nearly unchanged until reaching certain temperatures (10~20 K) and then an abrupt increase of ZFC M occurs. The different behaviors of un-doped Fe$_3$GaTe$_2$ and FNGT are due to the weak domain wall pinning of un-doped ones compared to that of doped crystals.[26] When the zero-field cools down and its volume is large enough, the FM material forms a multi-domain structure. For a pinning-type FM material, this multi-domain structure is fixed by domain wall pinning, and the domain walls are hardly moved by external stimuli. While the domain wall pinning of Fe$_3$GaTe$_2$ is easily depinned by a magnetic field applied during M–T measurement (1 kOe) and a marginal temperature increase, for FNGT with $x = 0.03$–0.12, ZFC M remains almost unchanged due to strong domain pinning until a certain temperature. When the temperature increases further, domain wall pinning is weakened by thermal energy, and suddenly the majority of domains are depinned and ZFC M drastically increases. After the abrupt increase of ZFC M, it increases gradually as the temperature increases up to T_C.

In Fig. 3e, the M of FNGT with $x = 0.22$ in the M–T curves with $H\parallel c$ significantly decreases compared to the M of $x = 0$–0.12 and T_C decreases to ~61 K. This indicates that the Ni dopants effectively suppress the FM characteristics of the crystal, reducing T_C to ~61 K. We expect that this FNGT with $x = 0.22$ is in the intermediate state between the FM state and the spin glass state, resulting in the suppression of domain pinning and rapid saturation behaviors. In Fig. 3f, the shape of the M–T curve indicates that the magnetic state of FNGT with $x = 0.68$ is the spin glass state.[5,6]

Fig. 4a–f show the M–H hysteresis loops at 2 K after zero-field cooling for FNGT with $x = 0$–0.68. In Fig. 4a, the H_c of un-doped Fe$_3$GaTe$_2$ is ~0.6 kOe, which shows pinning-type FM characteristics with a small H_d. As x is further increased up to $x = 0.12$, the hysteresis loop widens, which indicates the enhancement of H_c (Fig. 4b–d). When x reaches 0.22, H_c slightly decreases and a well-defined square-shaped hysteresis
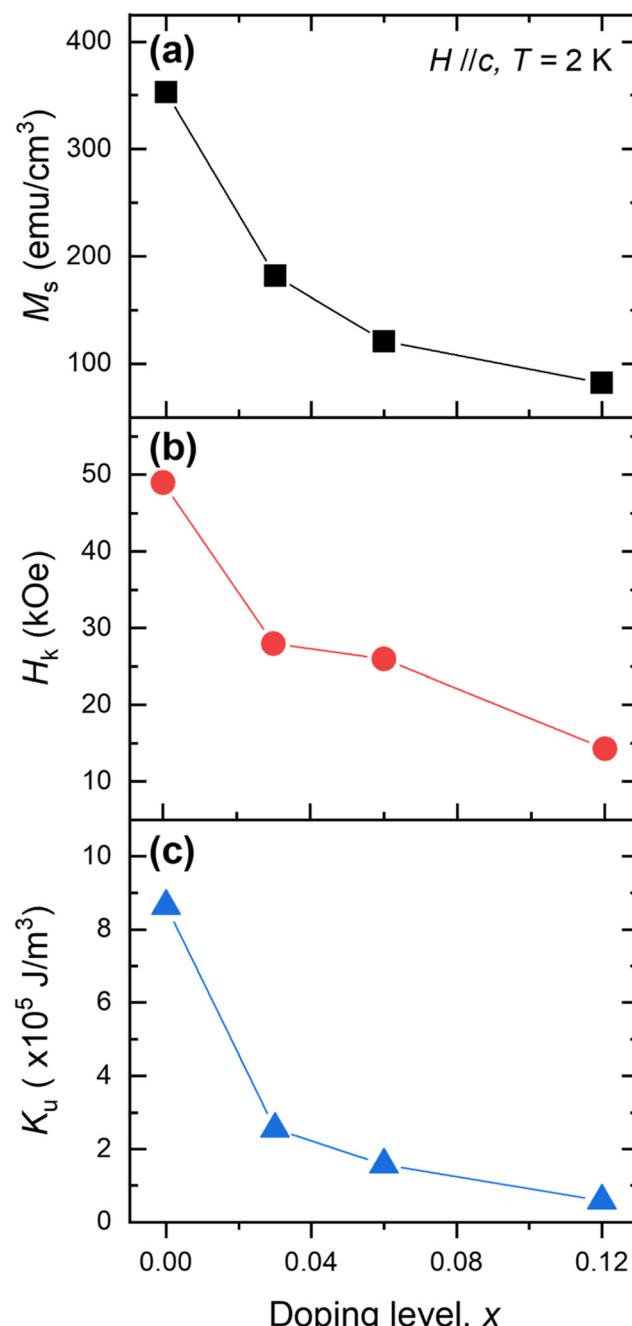
Fig. 5 Dopinglevel dependence of the FM characteristics of FNGT. (a) x dependence of the saturation magnetization (M_s) of FNGT. (b) x dependence of the anisotropy field (H_k) of FNGT. (c) x dependence of the anisotropy energy (K_u) of FNGT. All data are measured with $H\parallel c$ at 2 K.

loop is rounded as shown in Fig. 4e. A further increase of x results in the vanishing of FM characteristics, which shows a typical hysteresis loop of the spin glass state (Fig. 4f).[5,6] The H_c of each FNGT is plotted in Fig. 4g. The maximum H_c is 7 kOe from FNGT with $x = 0.12$, which is the highest H_c among those reported for vdW FM materials to date.

The ratio of remanent magnetization (M_r) to M_s for each crystal is plotted in Fig. 4h. When the M_r/M_s ratio of the un-doped crystal is 0.15, we can categorize it as a soft FM material like other Fe_xGeTe_2 systems.[11,12,26] For FNGT with $x = 0.03$, its M_r/M_s ratio is 0.98 whose value is very close to that of an ideal hard FM material. FNGT crystals with x up to 0.12 retain their hard FM characteristics, and then they gradually weaken as x increases further. Based on these results, we demonstrate that the H_c and M_r/M_s values are strongly Ni doping dependent, and that hard magnetic phases can be realized in the range of $0.03 \leq x \leq 0.12$.

The enhancement of H_c can originate from two factors.[30] One is the increase of K_u, which makes a FM system need more energy to flip the direction of its M. The other is the increase of domain wall energy and resultant domain pinning. To find out the origin of enhancement of H_c, we extracted the M_s and H_k values (presented in Fig. 5a and b) of FNGT with $x = 0$–0.12 from Fig. 2c, d and 4a–d. Then, we calculated K_u based on the following formula:

$$K_u = \frac{H_k M_{sat}}{2}.$$

As shown in Fig. 5c, K_u dramatically decreases with increasing x. A sudden decrease of K_u can be noted as the cause of the suppression of T_C,[13] but the enhancement of H_c cannot be explained with this result, as H_c decreases when K_u diminishes. Based on this observation, we attribute the enhancement of H_c to the increase of domain wall pinning induced by the insertion of Ni dopants.

In a FM system, flipping of entire M begins with flipping of local spins that need less energy to flip compared to adjacent spins due to, for example, an inhomogeneous environment. Once the magnetic field is applied, spins in the FM system initially resist the magnetic field up to H_c. When the strength of the magnetic field reaches H_c, spins that need less energy flip for aligning with the applied magnetic field, and adjacent un-flipped spins consecutively flip due to FM coupling between spins and Zeeman energy. This process continually occurs throughout the entire system, and this is the main reason that causes H_c to be smaller than H_k. The consecutive flipping process can be understood from the viewpoint of the domain wall motion in a multi-domain system. In this sense, the flipping process can be affected by factors that are related to the domain wall motion of a system. Fe atoms interact with adjacent Fe, Ga, and Te atoms and this interaction is the origin of long-range FM ordering. In FNGT, Ni dopants hinder the interaction between atoms as they may not interact effectively with neighboring atoms. As Ni dopants cancel out interactions around them, Ni sites naturally work as domain pinning sites. As x increases, more pinning sites are generated and the network strength of pinning sites is reinforced, which enhances H_c up to a record breaking value. A further increase of x increases non-magnetic Ni dopants and results in the suppression of FM characteristics of FNGT.

Fig. 6a shows the M–H hysteresis loops at 300 K after zero-field cooling for FNGT with $x = 0$–0.03. Even though the three-step M process observed from M–H at 2 K has become ambiguous, the H_c of FNGT with $x = 0.03$ is still higher than that of the un-doped one maintaining FM characteristics as shown in the inset of Fig. 6a and b. This result shows that the enhancement of H_c induced by Ni dopants can survive even above the room-temperature regime. Even though the H_c of pristine Fe_3GaTe_2 increases as the thickness decreases at low temperatures, the increase in H_c in thinner Fe_3GaTe_2 crystals at room temperature is negligible.[26] In contrast, it has been confirmed in our study that Ni doping enhances the H_c of bulk crystals by approximately 200% at room temperature. This enhancement may persist even in atomically thin crystals, resulting in a higher H_c for FNGT compared to that for pristine Fe_3GaTe_2 with the same thickness. Even a small amount of Ni dopant is expected to affect the H_c of Fe_3GaTe_2, and the enhancement of H_c in FNGT can be utilized for Fe_3GaTe_2-based spintronic devices that function in real-life environments.
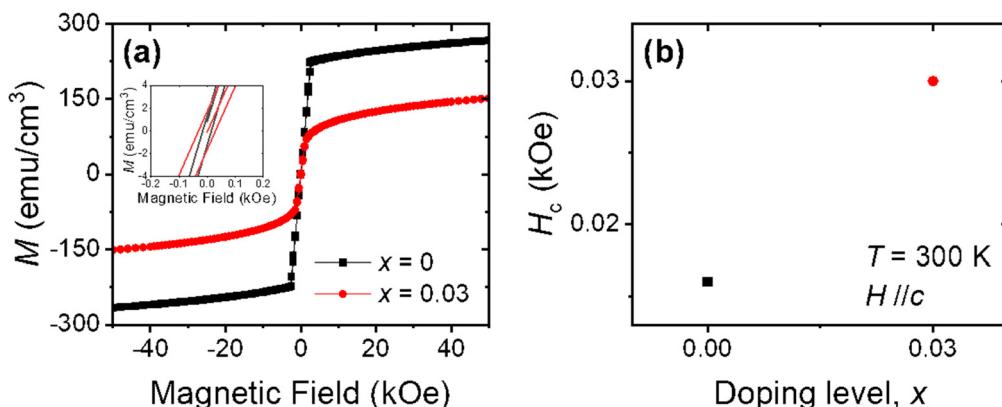
Fig. 6 Hysteresis loop of FNGT at 300 K. (a) Hysteresis loops of FNGT with $x = 0$ and 0.03 at 300 K. (b) x dependence of the H_c of FNGT at 300 K.

Conclusions

In this work, a metallic vdW ferromagnetic material FNGT with various doping levels from 0 to 0.68 was successfully synthesized. Even a small amount of Ni atom doping dramatically enhances the coercive field and affects its ferromagnetic characteristics, such as anisotropic energy and Curie temperature. In particular, the coercive field is enhanced by ∼1100% at a doping level of x = 0.12. The enhancement of the coercive field even persists above room temperature with an ∼200% increase. Our research not only suggests an effective way to control magnetic characteristics from the viewpoint of the coercive field but also proves the highly tunable magnetic characteristics of Fe_3GaTe_2 that are expected to make room temperature operating vdW spintronic devices possible.

Data availability

The data that support the findings of this study are available from the corresponding author upon request.

Author contributions

Hyo-Bin Ahn and Changgu Lee conceived the work. Hyo-Bin Ahn and Hyunjong Lim synthesized the crystals. Soon-Gil Jung and Tuson Park performed MPMS measurements. Hyo-Bin Ahn, Soon-Gil Jung, Kwangsu Kim, Sanghoon Kim, Tae-Eon Park, and Changgu Lee analyzed the data. Hyo-Bin Ahn, Soon-Gil Jung, Tuson Park, and Changgu Lee wrote the manuscript. All the authors discussed the results and commented on the manuscript.

Conflicts of interest

There are no conflicts to declare.

Acknowledgements

References

1 A. F. May, J. Q. Yan, R. Hermann, M. H. Du and M. A. McGuire, *2D Mater.*, 2022, **9**, 015013.

2 X. Chen, Y. T. Shao, R. Chen, S. Susarla, T. Hogan, Y. He, H. R. Zhang, S. Q. Wang, J. Yao, P. Ercius, D. A. Muller, R. Ramesh and R. J. Birgeneau, *Phys. Rev. Lett.*, 2022, **128**, 217203.

3 J. Seo, E. S. An, T. Park, S. Y. Hwang, G. Y. Kim, K. Song, W. S. Noh, J. Y. Kim, G. S. Choi, M. Choi, E. Oh, K. Watanabe, T. Taniguchi, J. H. Park, Y. J. Jo, H. W. Yeom, S. Y. Choi, J. H. Shim and J. S. Kim, *Nat. Commun.*, 2021, **12**, 2844.

4 C. K. Tian, F. H. Pan, S. Xu, K. Ai, T. L. Xia and P. Cheng, *Appl. Phys. Lett.*, 2020, **116**, 202402.

5 C. K. Tian, C. Wang, W. Ji, J. C. Wang, T. L. Xia, L. Wang, J. J. Liu, H. X. Zhang and P. Cheng, *Phys. Rev. B*, 2019, **99**, 184428.

6 G. Drachuck, Z. Salman, M. W. Masters, V. Taufour, T. N. Lamichhane, Q. S. Lin, W. E. Straszheim, S. L. Bud'Ko and P. C. Canfield, *Phys. Rev. B*, 2018, **98**, 144434.

7 R. R. Chowdhury, S. DuttaGupta, C. Patra, O. A. Tretiakov, S. Sharma, S. Fukami, H. Ohno and R. P. Singh, *Sci. Rep.*, 2021, **11**, 14121.

8 Z. Y. Li, M. Tang, J. W. Huang, F. Qin, L. Y. Ao, Z. W. Shen, C. R. Zhang, P. Chen, X. Y. Bi, C. Y. Qiu, Z. P. Yu, K. Zhai, T. Ideue, L. Wang, Z. Y. Liu, Y. J. Tian, Y. Iwasa and H. T. Yuan, *Adv. Mater.*, 2022, **34**, 2201209.

9 K. X. Zhang, S. Han, Y. Lee, M. J. Coak, J. Kim, I. Hwang, S. Son, J. Shin, M. Lim, D. Jo, K. Kim, D. Kim, H. W. Lee and J. G. Park, *Adv. Mater.*, 2021, **33**, 2004110.

10 J. Seo, D. Y. Kim, E. S. An, K. Kim, G. Y. Kim, S. Y. Hwang, D. W. Kim, B. G. Jang, H. Kim, G. Eom, S. Y. Seo, R. Stania, M. Muntwiler, J. Lee, K. Watanabe, T. Taniguchi, Y. J. Jo, J. Lee, B. I. Min, M. H. Jo, H. W. Yeom, S. Y. Choi, J. H. Shim and J. S. Kim, *Sci. Adv.*, 2020, **6**, eaay8912.

11 A. F. May, D. Ovchinnikov, Q. Zheng, R. Hermann, S. Calder, B. Huang, Z. Y. Fei, Y. H. Liu, X. D. Xu and M. A. McGuire, *ACS Nano*, 2019, **13**, 4436–4442.

12 C. Tan, J. Lee, S. G. Jung, T. Park, S. Albarakati, J. Partridge, M. R. Field, D. G. McCulloch, L. Wang and C. Lee, *Nat. Commun.*, 2018, **9**, 1554.

13 Y. J. Deng, Y. J. Yu, Y. C. Song, J. Z. Zhang, N. Z. Wang, Z. Y. Sun, Y. F. Yi, Y. Z. Wu, S. W. Wu, J. Y. Zhu, J. Wang, X. H. Chen and Y. B. Zhang, *Nature*, 2018, **563**, 94–99.

14 C. Hu, D. Zhang, F. G. Yan, Y. C. Li, Q. S. Lv, W. K. Zhu, Z. M. Wei, K. Chang and K. Y. Wang, *Sci. Bull.*, 2020, **65**, 1072–1077.

15 X. Wang, J. Tang, X. X. Xia, C. L. He, J. W. Zhang, Y. Z. Liu, C. H. Wan, C. Fang, C. Y. Guo, W. L. Yang, Y. Guang, X. M. Zhang, H. J. Xu, J. W. Wei, M. Z. Liao, X. B. Lu, J. F. Feng, X. X. Li, Y. Peng, H. X. Wei, R. Yang, D. X. Shi, X. Zhang, Z. Han, Z. D. Zhang, G. Y. Zhang, G. Yu and X. F. Han, *Sci. Adv.*, 2019, **5**, eeaw8904.

16 Z. Wang, D. Sapkota, T. Taniguchi, K. Watanabe, D. Mandrus and A. F. Morpurgo, *Nano Lett.*, 2018, **18**, 4303–4308.

17 Q. Li, M. M. Yang, C. Gong, R. V. Chopdekar, A. T. N'Diaye, J. Turner, G. Chen, A. Schol, P. Shafer, E. Arenholz, A. K. Schmid, S. Wang, K. Liu, N. Gao, A. S. Admasu,

S. W. Cheong, C. Y. Hwang, J. Li, F. Wang, X. Zhang and Z. Q. Qiu, *Nano Lett.*, 2018, **18**, 5974–5980.

18 K. Kim, J. Seo, E. Lee, K. T. Ko, B. S. Kim, B. G. Jang, J. M. Ok, J. Lee, Y. J. Jo, W. Kang, J. H. Shim, C. Kim, H. W. Yeom, B. I. Min, B. J. Yang and J. S. Kim, *Nat. Mater.*, 2018, **17**, 794–799.

19 T. X. Li, S. W. Jiang, N. Sivadas, Z. F. Wang, Y. Xu, D. Weber, J. E. Goldberger, K. Watanabe, T. Taniguchi, C. J. Fennie, K. F. Mak and J. Shan, *Nat. Mater.*, 2019, **18**, 1303–1308.

20 S. W. Jiang, L. Z. Li, Z. F. Wang, K. F. Mak and J. Shan, *Nat. Nanotechnol.*, 2018, **13**, 549–553.

21 B. Huang, G. Clark, D. R. Klein, D. MacNeill, E. Navarro-Moratalla, K. L. Seyler, N. Wilson, M. A. McGuire, D. H. Cobden, D. Xiao, W. Yao, P. Jarillo-Herrero and X. D. Xu, *Nat. Nanotechnol.*, 2018, **13**, 544–548.

22 M. Bonilla, S. Kolekar, Y. J. Ma, H. C. Diaz, V. Kalappattil, R. Das, T. Eggers, H. R. Gutierrez, M. H. Phan and M. Batzill, *Nat. Nanotechnol.*, 2018, **13**, 289–293.

23 C. Gong, L. Li, Z. L. Li, H. W. Ji, A. Stern, Y. Xia, T. Cao, W. Bao, C. Z. Wang, Y. A. Wang, Z. Q. Qiu, R. J. Cava, S. G. Louie, J. Xia and X. Zhang, *Nature*, 2017, **546**, 265–269.

24 M. W. Lin, H. L. L. Zhuang, J. Q. Yan, T. Z. Ward, A. A. Puretzky, C. M. Rouleau, Z. Gai, L. B. Liang, V. Meunier, B. G. Sumpter, P. Ganesh, P. R. C. Kent, D. B. Geohegan, D. G. Mandrus and K. Xiao, *J. Mater. Chem. C*, 2016, **4**, 315–322.

25 M. A. McGuire, H. Dixit, V. R. Cooper and B. C. Sales, *Chem. Mater.*, 2015, **27**, 612–620.

26 G. J. Zhang, F. Guo, H. Wu, X. K. Wen, L. Yang, W. Jin, W. F. Zhang and H. X. Chang, *Nat. Commun.*, 2022, **13**, 5067.

27 A. N. Kuznetsov, E. A. Stroganova, E. Y. Zakharova, A. V. Solopchenko, A. V. Sobolev, I. A. Presniakov, D. I. Kirdyankin and V. M. Novotortsev, *J. Solid State Chem.*, 2017, **250**, 90–99.

28 V. Jeudy, R. D. Pardo, W. S. Torres, S. Bustingorry and A. B. Kolton, *Phys. Rev. B*, 2018, **98**, 054406.

29 N. Leon-Brito, E. D. Bauer, F. Ronning, J. D. Thompson and R. Movshovich, *J. Appl. Phys.*, 2016, **120**, 083903.

30 B. J. Liu, Y. M. Zou, S. M. Zhou, L. Zhang, Z. Wang, H. X. Li, Z. Qu and Y. H. Zhang, *Sci. Rep.*, 2017, **7**, 6184.